A systematic comparison of ^{18}F-C-SNAT to established radiotracer imaging agents for the detection of tumor response to treatment

Timothy H Witney[1*], Aileen Hoehne[1*], Robert E Reeves[1], Ohad Ilovich[1], Mohammad Namavari[1], Bin Shen[1], Frederick T Chin[1], Jianghong Rao[1], Sanjiv S Gambhir[1]

[1]*Department of Radiology, Stanford University, Stanford, CA, USA*

**These authors contributed equally to this work*

Corresponding Author: Sanjiv Sam Gambhir, Department of Radiology, Stanford University, James H. Clark Center, 318 Campus Drive, E153 Stanford, CA 94305 USA. E-mail: sgambhir@stanford.edu; Tel: +1-650-725-2309

Financial support: This work was funded by NCI ICMIC P50 114747 and the Ben and Catherine Ivy Foundation.

Running title: Detection of tumor cell death by radionuclide imaging

Key words: Radiotracer, treatment response, cell death, comparison, C-SNAT

Word count: 4995

Figures: 6

Conflict of interest: None

Translational Relevance

Patients with similar tumor types frequently respond differently to the same therapy. An early assessment of treatment response in individual patients would allow rapid selection of the most effective treatment. Therapy response in the clinic currently relies on measurements of tumor size, which is ineffectual as an early response marker. In response, a number of positron emission tomography (PET) and single photon emission computed tomography (SPECT) radiotracers have been developed to noninvasively measure therapy-induced cell death a range of human cancers. Despite early promise, none of these imaging agents have made it into routine clinical practice. The development of new radiotracers to assess response to therapy are required if the goal of personalized medicine for the treatment of cancer is to be realized. Here, we designed a novel caspase 3-triggered cyclization and nanoaggregation radiotracer with improved sensitivity for the detection of cell death in comparison to current imaging gold standards.

ABSTRACT

Purpose: An early readout of tumor response to therapy through measurement of drug or radiation-induced cell death may provide important prognostic indications and improved patient management. It has been shown that the uptake of ^{18}F-C-SNAT can be used to detect early response to therapy in tumors by positron emission tomography via a mechanism of caspase 3-triggered nanoaggregation.

Experimental Design: Here, we compared the preclinical utility of ^{18}F-C-SNAT for the detection of drug-induced cell death to clinically evaluated radiotracers, ^{18}F-FDG, ^{99m}Tc-Annexin V and ^{18}F-ML-10 in tumor cells in culture, and in tumor-bearing mice *in vivo*.

Results: In drug-treated lymphoma cells, ^{18}F-FDG, ^{99m}Tc-Annexin V and ^{18}F-C-SNAT cell-associated radioactivity correlated well to levels of cell death ($R^2 > 0.8$; $P < 0.001$), with no correlation measured for ^{18}F-ML-10 ($R^2 = 0.05$; $P > 0.05$). A similar pattern of response was observed in two human NSCLC cell lines following carboplatin treatment. EL-4 tumor uptake of ^{99m}Tc-Annexin V and ^{18}F-C-SNAT were increased 1.4- and 2.1-fold, respectively in drug-treated *versus* naïve control animals ($P < 0.05$), although ^{99m}Tc-Annexin V binding did not correlate to *ex vivo* TUNEL staining of tissue sections. A differential response was not observed with either ^{18}F-FDG or ^{18}F-ML-10.

Conclusions: We have demonstrated here that ^{18}F-C-SNAT can sensitively detect drug-induced cell death in murine lymphoma and human NSCLC. Despite favorable image contrast obtained with ^{18}F-C-SNAT, the development of next generation derivatives, using the same novel and promising uptake mechanism, but displaying improved biodistribution profiles, are warranted for maximum clinical utility.

INTRODUCTION

The early assessment of drug-induced tumor cell death is of great prognostic value – enabling rapid selection of the most efficacious treatment using a personalized medicine approach. In the clinic, current methods to detect response rely on measuring changes in tumor size under the guidelines of the response evaluation criteria in solid tumors (RECIST) (1). This approach, however, lacks sensitivity, and many weeks may elapse before there is evidence on imaging of tumor volume shrinkage.

Cell death, through apoptotic, necrotic or alternate pathways (3), is the surrogate endpoint for most anticancer therapies and treatments (4, 5). Given the inadequacy of current techniques for monitoring drug response, there have been considerable efforts to develop new techniques to detect and image treatment efficacy through measurements of tumor cell death (recently reviewed in (6)). As drug-induced cell death manifests itself in many different forms, numerous divergent imaging strategies have been employed, targeting a range of both direct and indirect biomarkers. Direct imaging biomarkers include caspase 3, whose activation commits the cell to programmed (apoptotic) cell death (7, 8), and plasma membrane depolarization (9, 10), which occurs downstream of caspase 3 (11) or is exposed as a result of membrane rupture during necrosis (9). Indirect methods include measurements of cell metabolism (12, 13), the release of enzymes from intracellular compartments (14, 15), or the increased diffusion of water that results from loss of cellularity (16).

Radiotracer imaging techniques have shown great promise for the non-invasive detection of cell death. Early alterations in glucose metabolism following therapy, characteristic of both stressed

and dying cells, have been detected by 2-^{18}F-fluoro-2-deoxy-D-glucose (^{18}F-FDG) positron emission tomography (PET) in a range of tumor types (17-20). Furthermore, a draft framework has been proposed for the routine use of ^{18}F-FDG-PET for response-assessment in the clinic (21). In addition to ^{18}F-FDG, the small molecule radiotracer 2-(5-fluoropentyl)-2-methyl malonic acid (^{18}F-ML-10) has shown utility for cell death imaging pre-clinically (22, 23), with first-in-man trials recently reported (24). Out of all the currently available cell death imaging probes, ^{99m}Tc-HYNIC-labelled Annexin V (^{99m}Tc-Annexin V) has been the most widely studied, having been used to image drug-induced cell death in human head and neck squamous cell carcinoma (25) and tumors of the breast, lymphoma and lung (26). ^{99m}Tc-Annexin V binds to phosphatidylserine (PS), a temporally-stable biomarker exposed following either apoptotic or necrotic cell death. ^{99m}Tc-Annexin V, however, has failed to progress beyond phase II/III clinical trials due to its poor biodistribution profile (27).

Despite the promise of non-invasive imaging techniques for the assessment of tumor cell death, no imaging agent has yet been accepted into routine clinical practice. This has prompted the development of a new generation of agents designed to monitor response. One such radiotracer, ^{18}F-C-SNAT, has been shown in preliminary studies to detect early response to therapy in tumors by PET via a novel mechanism of caspase 3-triggered cyclization and nanoaggregation ((8); Supplemental Fig. S1). Here, we directly compared the performance of ^{18}F-C-SNAT to established radiotracers, ^{18}F-FDG, ^{99m}Tc-Annexin V and ^{18}F-ML-10 (Fig. 1), for the non-invasive detection of cell death. We found that all radiotracers except ^{18}F-ML-10 were able to sensitively measure drug-induced cell death in cell culture. However, only ^{18}F-C-SNAT was able

to measure treatment response *in vivo*. Together, our analysis suggests that ^{18}F-C-SNAT may have utility for the detection of drug-induced cell death in the clinic.

MATERIALS AND METHODS

Cell culture

EL-4 murine lymphoma cells and PC-9 human NSCLC (ATCC) were grown in complete RPMI medium (Life Technologies; 11.1 mM glucose), supplemented with 10% fetal calf serum, 100 U/mL penicillin, and 100 μg/mL streptomycin. A549 cells (ATCC) were grown in DMEM medium (Life Technologies; 25 mM glucose) with 10% fetal calf serum, 100 U/mL penicillin, and 100 μg/mL streptomycin. All cells were propagated at 37°C in a humidified atmosphere containing 5% CO_2. EL-4 cells could not be authenticated as they were of non-human origin, with A549 and PC-9 cells purchased from an authenticated cell biobank just prior to publication.

Radiotracers

Radiosynthesis of ^{18}F-FDG, ^{99m}Tc-Annexin V, ^{18}F-ML-10 and ^{18}F-C-SNAT was based on previously described methodology, as detailed in the supplemental materials.

Cell uptake studies

18 – 20h post either etoposide (Sigma-Aldrich; 15 μM) or vehicle treatment (DMSO), EL-4 cells were split into two fractions for analysis: 1. Assessment of radiotracer cell uptake and binding. 2. Cell death determination by flow cytometry. For cell uptake studies, 10^6 EL-4 cells were incubated for 10, 30 or 60 min in fresh RPMI (1 mL) at 37 °C with respective radiotracer to

determine uptake kinetics. PC-9 and A549 cells were seeded at 10^5 cells/well of a 6-well plate 24h prior to carboplatin treatment (Sagent; 200 µM; 72h), as previously described (28). For all cell uptake experiments, the radiotracers were added at the following concentrations and specific activities: ^{18}F-FDG, 0.185 MBq/mL, <0.38 ± 0.08 µM, >2.6 GBq/µmol; ^{99m}Tc-Annexin V, 10 nM, ~0.185 MBq/mL, 21.1 ± 2.2 GBq/µmol; ^{18}F-ML-10, 1.48 MBq/mL, <0.18 µM, >7.4 GBq/µmol; ^{18}F-C-SNAT, 1.48 MBq/mL, 0.015 ± 0.007 µM, 123.2 ± 61.4 GBq/µmol. Following incubation for the allotted time, adherent cells were trypsinized (0.25% trypsin; 1 mM EDTA) and harvested by centrifugation (1200 *g*; 3 min; 4°C). Detached cells present in the media before trypsinization were retained and pooled with the trypsinized cells. Suspension cells were collected by centrifugation (1200*g*; 3 min; 4°C), and all cells were washed three times with ice-cold Hank's Buffered Salt Solution (HBSS; 1 mL; 1200 *g;* 3 min; 4°C), with the final cell pellet lysed in 200 µL RIPA buffer (Thermo Fisher Scientific Inc). 100 µL cell lysates were transferred to counting tubes and decay-corrected radioactivity was determined on a gamma counter (Cobra II Auto-Gamma counter, Packard Biosciences Co). The remaining lysate was frozen and used for protein determination following radioactive decay using a bicinchoninic acid (BCA) 96-well plate assay (Thermo Fisher Scientific Inc.). 10 µL standards from the original non-washed cell/media suspension were counted to quantitate the percentage of radiotracer uptake/binding in cells.

To correlate cell-associated radioactivity with levels of drug-induced cell death, mixtures of vehicle and etoposide-treated EL-4 cells were prepared 18 – 20h post either vehicle or drug addition. Mixtures contained 0%, 25%, 50%, 75% and 100% *v*/*v* etoposide-treated cells in 6 mL total volume, with the remaining volume made from vehicle-treated cell suspension. One million

cells were subsequently collected for cell death analysis by flow cytometry, with the remaining cells used to assess cell-associated radioactivity 60 min post radiotracer addition, as described above.

Detection of Cell Death *In Vitro*

Apoptosis and necrosis in cell mixtures containing 0 – 100% drug-treated cells were visualized by flow cytometry using a method adapted from (13), in parallel to cell uptake studies. Fluorescein isothiocyanate (FITC)-Annexin V (BioLegend) in combination with 7-amino-antinomycin D (7-AAD; BioLegend) were used for cell death determination. Early apoptotic cells were defined as cells positively stained for FITC-Annexin V but not 7-AAD, with both late apoptotic and necrotic classified as cells positive for both stains. FlowJo (v.7.6.5, Tree Star, Inc.) was used for analysis.

***In vivo* tumor models**

All experimental procedures involving animals were approved by Stanford University Institutional Animal Care and Use Committee. EL-4 tumor cells (5×10^6 in 100 µL PBS) were injected subcutaneously on the back of female C57BL/6 mice (aged 6 – 8 weeks; Charles River Laboratories) and grown to ~150 mm^3, over ~6 days. Tumor dimensions were measured daily using a caliper, with tumor volumes calculated by the equation: volume = $(\pi / 6) \times a \times b \times c$, where *a*, *b*, and *c* represent three orthogonal axes of the tumor (28). At day 6, animals were size-matched and either treated with clinically-formulated etoposide (Topsar, Novaplus; 70 $mg.kg^{-1}$) or left untreated. Treatment-response analysis was performed 24h post drug treatment, 7 days post tumor cell implantation. In a separate cohort of mice, the effect of drug-treatment on tumor

volume was followed up to 96h post therapy. For all other experiments, animals were culled 25.5h post therapy and tissues excised for analysis.

Imaging studies

PET imaging scans were carried out on a docked Siemens Inveon PET/CT scanner (matrix size, 128 × 128 × 159; CT attenuation-corrected; non-scatter corrected), following a bolus *i.v.* injection of ~10 MBq of the radiotracer into tumor-bearing mice (n = 3 – 4 per group). Dynamic scans were acquired in list mode format over 90 min, as described in detail in the supplemental materials.

Biodistribution studies

~10 MBq of radiotracer was injected via the tail vein of anaesthetized EL4 tumor-bearing C57BL/6 mice (n = 4 – 8 per group). These mice were maintained under anesthesia and warmed to 37°C to replicate imaging conditions. At 90 min post radiotracer injection, animals were sacrificed by exsanguination via cardiac puncture. For all animals, tumors were excised immediately upon death, weighed and rapidly placed in 10% formalin (Fisher Scientific) for fixation. Tumor and tissue radioactivity was subsequently determined on a gamma counter (decay-corrected; Cobra II Auto-Gamma counter, Packard Biosciences Co). Predefined 3.7 MBq standards (250 µL) were also counted for data normalization to injected dose. Data were expressed as percent injected dose per gram of tissue (%ID/g).

Immunohistochemistry

Formalin-fixed tumors were embedded in paraffin, sectioned into 5 µm-thick slices and placed on microscope slides according to standard procedures (Histo-Tec Laboratory). Sections were taken at regular intervals across the entire tumor volume in order to capture previously described heterogeneity of EL-4 tumors (29). Sections were stained with either hematoxylin and eosin (H&E; Histo-Tec) with a colorimetric TdT-mediated dUTP Nick-End Labeling (TUNEL) assay using a kit by Promega (DeadEnd™), according to the manufacturer's instructions and each section digitized using a NanoZoomer 2.0RS whole-slide scanner (Hamamatsu). The percentage are of TUNEL-positive cells was measured across the entire tumor section using ImageJ (v.1.47; National Institutes of Health). 6 sections were analyzed per tumor, with 3 tumors evaluated per treatment group (naïve or drug-treated) for each radiotracer studied. TUNEL positivity was compared to the corresponding tumor uptake values previously determined by biodistribution.

Statistical analysis

Data were expressed as mean ± SD, with the exception of tumor volume measurements, which were presented as mean ± SEM. Statistical significance was determined using the Student *t* test (Microsoft Excel). For correlation analysis, linear regression, statistical significance and 95% confidence levels were determined using Prism software for Mac OS X (v.6.0e; GraphPad Software). Differences between groups were considered significant if $P \leq 0.05$.

RESULTS

Measurements in cells

Time course of radiotracer accumulation

EL-4 murine lymphoma cells rapidly undergo caspase 3-mediated cell death following etoposide treatment (13). By 18h post therapy, cell death had reached 48.9 ± 6.7% in comparison to 2.6 ± 1.4% in vehicle-treated cells, as determined by flow cytometry (Fig. 2A; $P < 0.001$; $n = 4$). Temporal ^{18}F-FDG, ^{99m}Tc-Annexin V, ^{18}F-ML-10 and ^{18}F-C-SNAT uptake/cell binding was measured at 18 – 20h post drug treatment to permit the comparison of their uptake kinetics (Fig. 2B). ^{18}F-FDG cell uptake increased linearly with time in vehicle-treated cells, rising from 3.1 ± 1.2% radioactivity/mg protein at 10 min post radiotracer addition, to 10.7 ± 2.2% radioactivity/mg protein by 60 min. In comparison, ^{18}F-FDG uptake in drug-treated cells at 60 min was 2.0 ± 0.7% radioactivity/mg protein, 5.3-fold lower than vehicle controls ($n = 4$; $P = 0.0008$). Conversely, high ^{99m}Tc-Annexin V binding to drug-treated cells was evident by just 10 min post radiotracer addition, at 110.4 ± 4.0% radioactivity/mg protein, with significantly lower binding measured in vehicle controls (6.0 ± 1.9% radioactivity/mg protein; $P < 0.001$; $n = 3$). By 60 min post radiotracer addition, ^{99m}Tc-Annexin V binding was 24.3-fold higher in drug-treated *versus* vehicle-control cells, at 173.2 ± 15.7% radioactivity/mg and 7.1 ± 2.4% radioactivity/mg, respectively ($P < 0.001$; $n = 3$). No difference in EL-4 cell uptake in treated *versus* control cells was detectable with ^{18}F-ML-10 over the 60 min time course ($P > 0.05$; $n = 3$). Cell-associated radioactivity at 60 min in etoposide-treated cells was 3-orders of magnitude lower than ^{99m}Tc-Annexin V, at 0.10 ± 0.04% radioactivity/mg. ^{18}F-C-SNAT retention in drug-treated cells followed an initial phase of slow uptake for the initial 30 min, followed by a rapid increase in the rate of retention over the proceeding 30 min. There was no change in ^{18}F-C-SNAT cell uptake in vehicle control cells over the 60 min time course. At 60 min, ^{18}F-C-SNAT cell uptake was 4.5-

fold higher in drug-treated cell in comparison to vehicle controls, at 1.5 ± 0.2% radioactivity/mg and 0.3 ± 0.1% radioactivity/mg, respectively ($P < 0.001$; $n = 3$).

Correlation to cell death

Radiotracer uptake and EL-4 cell binding were further compared to levels of drug-induced cell death in culture. Here, different ratios of drug-to-vehicle treated cells were combined to create a large dynamic range of dying cells, from ~3–80% of the total cell population (Fig. 3). As both early and late apoptotic/necrotic cells were present in the drug-treated samples used to prepare the sample series (Supplementary Fig. S2), it was impossible to determine the contribution of each mechanism of death to cell uptake using this method. Instead, cell-associated radioactivity was compared to cells identified as positively stained by FITC-Annexin V, defined here as 'dying cells'. Both ^{99m}Tc-Annexin V and ^{18}F-C-SNAT cell uptake/binding significantly correlated with levels of cell death ($R^2 = 0.985$ and 0.924, respectively; $P < 0.001$), with ^{18}F-FDG uptake negatively correlated to death ($R^2 = 0.842$; $P < 0.001$). There was no statistically significant correlation found for ^{18}F-ML-10 ($R^2 = 0.053$; $P > 0.05$). It is important to note that ^{99m}Tc-Annexin V was correlated to a fluorescent Annexin V derivative used for the assessment of cell death; a potential limitation of this comparison.

Monitoring therapy response in NSCLC

To explore whether the radiotracer uptake results in EL-4 lymphoma cells were generalizable to other tumor cell lines taken from solid tumors, we next assessed radiotracer uptake in either vehicle or carboplatin-treated human PC-9 and A549 NSCLC cells; a tumor type well known for its relative resistance to common chemotherapeutics (30). 72h carboplatin treatment induced

extensive cell death in both lines (Supplementary Fig. S3A). In PC-9 and A549 cells, drug treatment resulted in a significant 69.8% ($P < 0.001$; $n = 3$) and 43.9% ($P = 0.01$; $n = 3$) reduction in ^{18}F-FDG uptake 60 min post radiotracer addition (Supplementary Fig. S3B). For ^{99m}Tc-Annexin V, radioactivity was increased 5- and 4-fold in PC-9 and A549 cells, respectively in comparison with vehicle control cells ($P < 0.001$; $n = 3$). Similarly, ^{18}F-C-SNAT was increased 3.8-fold ($P = 0.03$) and 2.9-fold ($P < 0.001$) in PC-9 and A549, respectively ($n = 3$). For ^{18}F-ML-10, no significant increase observed in drug-treated cells *versus* vehicle for either PC-9 or A549 cells, in agreement with data obtained for EL-4 cells.

Monitoring treatment response in tumors

We next evaluated the specificity of each radiotracer to non-invasively measure tumor cell death *in vivo*. Subcutaneous EL-4 tumors grew rapidly in C57BL/6 mice, detectably by day 4 and reaching ~150 mm^3 six days post-implantation (Fig. 4A). On day 6 mice were size matched and either treated with drug or left untreated. Drug treatment resulted in a significant 40% reduction in tumor volume after 24h, reduced from 159.8 ± 26.3 mm^3 to 95.3 ± 16.0 mm^3, whereas the tumor volume increased from 145.3 ± 23.2 mm^3 to 256.4 ± 36.3 mm^3 in naïve animals (80% increase; $P < 0.001$; $n = 7$/group). At this time point, drug-treated tumors were characterized by loss of tumor cellularity, immune cell infiltration (Fig. 4B) and extensive DNA damage throughout multiple slices of the tumor, determined by histochemical staining (Fig. 4C). In naïve tumor-bearing animals, DNA damage was limited to the peripheral margins of the tumor. By 96h post therapy, tumors had shrunk to 42.8 ± 7.2 mm^3, growing to 393.4 ± 23.2 mm^3 in naïve animals (Fig. 4A).

Tumor uptake and radiotracer biodistribution

^{18}F-FDG, ^{99m}Tc-Annexin V, ^{18}F-ML-10 and ^{18}F-C-SNAT tumor uptake, illustrated in Figure 4D, and *ex vivo* biodistribution profiles, summarized in Supplemental Table 1, were measured in EL-4 tumor-bearing animals 90 min post radiotracer injection in either drug-treated or naïve animals. ^{18}F-FDG, ^{99m}Tc-Annexin V and ^{18}F-ML-10 pharmacokinetics were dominated by renal excretion. In addition, high heart and kidney retention were measured with ^{18}F-FDG and ^{99m}Tc-Annexin V, respectively. ^{18}F-C-SNAT elimination was through both the renal and hepatobiliary routes. ^{18}F-ML-10 radioactivity had almost completely cleared from all organs by 90 min. For drug-treated mice, ^{18}F-FDG was significantly higher than naïve animals in liver, small intestine and large intestine, but lower in muscle ($P < 0.05$). Bone-associated radioactivity was significantly higher in treated *versus* naïve animals with ^{99m}Tc-Annexin V ($P < 0.05$).

Ex vivo γ-counting of excised tumors revealed a significant increase in tumor-associated radioactivity in drug-treated versus naïve tumor-bearing mice for both ^{99m}Tc-Annexin V and ^{18}F-C-SNAT, at 1.4- and 2.1-fold, respectively ($P < 0.05$; $n = 4 – 7$ mice/group). There was no change in ^{18}F-FDG or ^{18}F-ML-10 tumor uptake and retention following drug treatment 90 min post injection of radiotracer (Fig. 4D and Supplemental Table 1). A positive tumor-to-muscle ratio was measured with all radiotracers and treatment conditions, whereas a positive tumor-to-blood ratio was only measured with ^{18}F-FDG at 90 min post-radiotracer injection (Supplemental Table 2).

Correlation of radiotracer binding to histology

The specificity of the radiotracers to image tumor response to therapy was achieved through correlation of their retention with TUNEL staining, an independent marker of drug efficacy and the current clinical gold standard (Fig. 5). EL-4-tumor bearing animals injected with ^{18}F-C-SNAT showed a good correlation (R^2 = 0.778; *n* = 3 animals/group; *P* = 0.02) between whole tumor mean radioactivity at 90 min post radiotracer injection and TUNEL staining in histological sections obtained post mortem, whereas there was no correlation for either ^{18}F-FDG, ^{99m}Tc-Annexin V or ^{18}F-ML-10 (R^2 = 0.249, 0.231 and 0.001, respectively; *n* = 3 animals/group; P > 0.05).

Radionuclide imaging of tumor cell death

Dynamic PET images were acquired from animals with implanted EL-4 tumors (Fig. 6). Similarly to *ex vivo* biodistribution data, ^{18}F-FDG distribution was characterized by high uptake in the tumor, heart and bladder (Fig. 6A). ^{18}F-FDG-PET/CT fusion images, highlighting the tumor xenograft and rendered in 3D, are shown in Figure 6A(ii) (full, uncropped versions are displayed in Supplementary videos M1 and M2). ^{18}F-FDG tumor uptake was characterized by a steady increase in tumor retention in both naïve and drug-treated animals, with a plateauing of radioactivity recorded between 60 – 90 min. By 90 min a significant increase in tumor-associated ^{18}F-FDG uptake was measured in drug-treated animals in comparison to naïve animals at 15.1 ± 1.2 %ID/g and 12.3 ± 1.1 %ID/g, respectively (*P* = 0.011; *n* = 4/group). There was no difference in the area under the tumor time-activity curves (AUC) between the two treatment groups (*P* > 0.05).

Tumor uptake and retention was visible above background in both naïve and drug-treated animals with ^{18}F-ML-10 PET (Fig. 6B), with increased uptake noticeable around the periphery of the tumor (Fig. 6B(ii), Supplemental videos M3 and M4). The kinetic profile of tumor retention varied considerably for ^{18}F-ML-10 in comparison to ^{18}F-FDG, as shown by the tumor time-activity curves (TAC). Rapid tumor uptake of ^{18}F-ML-10, peaking at 10 minutes, preceded a slow washout of radioactivity over the remaining 80 minutes. There was no difference in image-derived tumor uptake values (%ID/g_{90} or AUC) between naïve and drug-treated cohorts.

In contrast to what was observed with ^{18}F-ML-10 and ^{18}F-FDG-PET, a clear difference in tumor-associated ^{18}F-C-SNAT uptake between treatment groups was measured by PET (Fig. 6C). In drug-treated mice, background activity was increased when compared to naïve mice, possibly reflecting the trend towards increased blood retention observed in biodistribution studies (Supplemental Table 1). In naïve mice, tumor uptake was confined to the margins (Fig. 6C(ii) and Supplemental video M5), corresponding to elevated regions of DNA damage observed by histochemical staining of excised tumors (Fig. 4C), whereas uniform tumor distribution was evident in tumors of drug-treated mice (Fig. 6C(ii) and Supplemental video M6). The profile of tumor uptake varied considerably between drug-treated and naïve animals (Fig. 6C(iii)). In drug-treated animals, C-SNAT rapidly accumulated in tumors, peaking at 10 minutes, with subsequent stabilization of tumor-associated radioactivity. For naïve animals, ^{18}F-C-SNAT peaked to similar levels 10 minutes post injection, followed by a slow washout from the tumor over the remaining 80 minutes. By 90 min post injection, tumor uptake was 2.2 ± 0.2 %ID/g in drug-treated tumors *versus* 0.8 ± 0.2 %ID/g when left untreated, a 2.7-fold increase ($P < 0.001$, n = 3-4 animals/group).

Dynamic SPECT imaging was not possible with the experimental setup available. Instead, static 60 – 90 min SPECT images were obtained for ^{99m}Tc-Annexin V (Supplemental Fig. S4). These images revealed typical ^{99m}Tc-Annexin V tissue distribution, with high liver, kidney and bladder radioactivity, which was consistent with biodistribution data. Although tumor uptake was evident above background, we were unable to distinguish between drug-treated tumors and naïve controls using qualitative imaging data alone, reflecting the small differences observed by *ex vivo* γ-counting.

DISCUSSION

Resistance to chemotherapy and molecularly-targeted therapies provides a major hurdle for cancer treatment due to the underlying genetic and biochemical heterogeneity of tumors. An early read-out of drug efficacy, through the measurement of tumor cell death, would provide valuable insights into resistance status, allowing the selection of the most appropriate therapy (or combination) for the individual and termination of ineffectual treatments at an early stage.

There have been considerable efforts to develop methods to non-invasively measure tumor cell death (recently reviewed in (6)), but as yet, no cell-death imaging agent has made it into routine clinical practice. There is therefore a need to develop new imaging agents for the assessment of therapy response. A number of important considerations are required to assess the suitability for any novel cancer imaging agent: namely, the temporal and spatial distribution of the imaging biomarker in tumors, the sensitivity and specificity of detection, tumor-to-background contrast and the pharmacokinetic profile of the radiotracer. Here, we systematically compared the novel

imaging agent, ^{18}F-C-SNAT, to clinically evaluated radiotracers, ^{18}F-FDG, ^{18}F-ML-10 and ^{99m}Tc-Annexin V, for the detection of tumor cell death. We selected the well-characterized EL-4 murine lymphoma model (12-14) for the assessment of drug-induced cell death. Lymphomas typically respond well to first-line therapy in comparison to the majority of solid tumor types (31), accurately reflected by extensive drug-induced cell death observed here in EL-4 cells and in implanted tumors (Fig. 2A and 4A – C, respectively). We then further assessed therapy response in two additional NSCLC lines to confirm that the variability in results between the different radiotracers was not specific to this one cell line.

In cell culture experiments, EL-4 cell-associated radioactivity for the different radiotracers varied over 3 orders of magnitude following drug treatment (Fig. 2), highlighting large differences in their sensitivity and mechanisms to detect cell death. For ^{99m}Tc-Annexin V, cell-associated radioactivity was 173.2 ± 15.7% radioactivity/mg protein at 60 min post addition of radiotracer, in comparison to just 0.10 ± 0.04% radioactivity/mg for ^{18}F-ML-10. Furthermore, ^{18}F-ML-10 uptake failed to correlate to drug-induced cell death in this model, either in cells or in tumors (Fig. 3 and 5, respectively); a pattern also replicated in the two NSCLC cells tested here. This is in contrast to previous reports in a preclinical model of neuronal cell death (27) and in drug-treated tumor cells in culture, in which a tritiated derivative of ML-10 was used (32). It is possible that tissue culture media buffering of extracellular pH may reduce cell binding of ^{18}F-ML-10, whose binding is purportedly mediated through the acidification of the external plasma membrane leaflet (32). Experimental evidence linking apoptosis-specific alterations in asymmetric membrane distribution to ^{18}F-ML-10 uptake is limited however, and not supported

by our findings *in vivo*, where the acidic tumor microenvironment likely remains largely un-buffered (14).

Drug treatment induced high levels of DNA damage and loss of cellularity *in vivo*, characteristic of an apoptotic response. Despite the high levels of cell death, accumulation in EL-4 tumors was moderate (<3 %ID/g) for all radiotracers except ^{18}F-FDG (Fig 4C and 6A). A significant decrease in ^{18}F-FDG uptake is indicative of a positive response to therapy, as measured here in EL-4 cells (Fig 2B and 3), as a consequence of glucose transporter redistribution from the plasma membrane to the cytosol (13). Despite levels of drug-induced cell death correlating excellently with a reduction in ^{18}F-FDG uptake in cells, no response was detectable by γ-counting of excised tumors *ex vivo* (Fig. 4D and 5), with a small but statistically significant increase observed by semi-quantitative imaging parameters *in vivo*. ^{18}F-FDG uptake is not confined to tumor cells, with drug-induced alterations in other constituents of the tumor microenvironment potentially confounding measurements *in vivo*. For example, infiltration of FDG-avid immune cells following drug treatment, detected here by H&E staining (Fig. 4B), may mask tumor cell-specific reductions in glucose metabolism in this immuno-competent murine model, as has been observed elsewhere (33, 34). These data are in line with the general advice for nuclear medicine physicians to wait a minimum of 10 days after chemotherapy before performing ^{18}F-FDG-PET scans to bypass potential immune effects (21). A reduction in ^{18}F-FDG in lymphoma patients has however been observed just 24h post initiation of treatment (35) highlighting a potential limitation of preclinical mouse models of cancer, where the nature and timing of immune responses are known not to precisely match those found in the clinic (36).

While changes in ^{18}F-FDG uptake act as an indirect measure of treatment response, Annexin V and its labeled derivatives have been shown to measure *bona fide* cell death, through binding to exposed PS with nanomolar affinity (37). Annexin V continues to be the gold standard for measurements of cell death *in vitro*. In culture, ^{99m}Tc-Annexin V binding excellently correlated to cell death, with high sensitivity and specificity in both the lymphoma and two NSCLC cell lines. Despite encouraging performance in cell culture, a poor pharmacokinetic profile and low tumor binding was observed *in vivo*. The half-life of ^{99m}Tc (6 h) permits imaging at time points over 12h post radiotracer injection. The rapid clearance of ^{99m}Tc-Annexin V from circulation and absence of tissue redistribution just 30 min post injection (38) however supports an imaging protocol whereby response is assessed at 90 min post-intravenous injection. At this time point, ^{99m}Tc-Annexin V tumor uptake did not correlate significantly to levels of DNA damage (Fig. 5), with a modest 40% increase in radioactivity accumulation following drug treatment detectable by average counts in excised tumors. Non-specific tumor retention of Annexin V in the vascular space has recently been attributed to changes in enhanced permeability and retention (EPR) effects at baseline and post therapy (39). Despite advances in both site-specific and PET labeling strategies little has been achieved to improve the *in vivo* profile and tumor binding of this radiotracer (40).

Given the relatively poor performance of existing radiotracers, alternative approaches are required for the measurement of cell death. PET-labeled and fluorescent derivatives of a peptidic caspase 3/7 substrate, C-SNAT and C-SANF, respectively, have recently emerged as promising agents for cell death imaging (8, 41). Specificity of C-SNAT for caspase 3/7 was previously shown, through abrogation of signal in the presence of a caspase 3 inhibitor, and with a control

probe containing the D-DEVD sequence, resistant to caspase 3 cleavage (8, 41). Here, ^{18}F-C-SNAT uptake was significantly elevated between 2.9- and 4.5-fold in EL-4 and NSCLC cells following treatment. In EL-4 xenograft tumors, ^{18}F-C-SNAT uptake correlated strongly with the levels of drug-induced DNA damage (R^2 = 0.778), with ^{18}F-C-SNAT uptake increased 2.7-fold in drug-treated tumors *versus* naïve controls just 24h post therapy. This early readout of treatment response was shown to be an accurate predictor of outcome, assessed by almost complete tumor regression 72h post therapy (Fig. 4A). At 90 min post radiotracer injection, washout of unbound radiotracer in muscle resulted in a positive tumor-to-muscle ratio in both drug-treated and naïve mice. Retention of the radiotracer in the blood pool combined with relatively low tumor uptake however reduced tumor-to-background contrast and may confound simple endpoint measurements, particularly for the evaluation of vascular-damaging anticancer agents where radiotracer delivery to the tumor may be impaired. Of note was the combined hepatobiliary and renal excretion of ^{18}F-C-SNAT, which may limit assessment of treatment response to tumors of the upper thoracic region, for example, those of the breast, in which background is minimal. We are currently developing second-generation caspase 3-mediated nanoaggregation radiotracers with improved pharmacokinetic properties, and improved signal to background for enhanced clinical utility.

Not included in this comparison study was the PET-labeled caspase 3 inhibitor, isatin-5-sulfonamide (^{18}F-ICMT-11), which has shown potential for tumor cell death imaging (7, 28, 42) and has recently progressed to clinical trials (43). Under similar conditions to those described here however, EL-4 tumor retention of ^{18}F-ICMT-11 was increased by a modest 65% in treated *versus* vehicle control tumors (44), whilst sharing the same suboptimal pharmacokinetic profile

as ^{18}F-C-SNAT, and displaying lower tumor binding *in vivo* (42). A potential limitation of caspase 3-based imaging agents, such as ^{18}F-C-SNAT and ^{18}F-ICMT-11, is the transient temporal expression of cleaved caspase 3 following the induction of apoptosis. As a result, the imaging window for the detection of treatment response must be carefully selected for these caspase 3-based imaging agents (42). In addition, measurements of caspase 3 limits detection to apoptotic mechanisms of death and fails to detect therapy-induced necrosis (28).

In summary, we have systematically compared a range of radionuclide imaging agents, with diverse mechanisms of action, for cell death imaging. Despite promising results obtained in isolated adherent and suspension cells in culture, confounding factors *in vivo*, such as microenvironmental changes and radiotracer biodistribution, limited the ability of both ^{99m}Tc-Annexin V and ^{18}F-FDG to sensitively measure cell death. The claimed selectivity of ^{18}F-ML-10 to monitor treatment response could not be replicated in the EL-4 tumor model in the current work. Whilst progress has been made with the development of novel PET agents, such as ^{18}F-C-SNAT, there is an urgent need to continue to develop new radiotracers which display an improved pharmacokinetic profile and tumor uptake in order to measure treatment response of tumors located in the abdomen and surrounding regions. Furthermore, detailed clinical studies will be needed to truly identify a radiotracer that can have utility in monitoring treatment efficacy.

ACKNOWLEDGEMENTS

We would like to thank Francis Blankenberg for provision of reagents and for helpful comments relating to the preparation and evaluation of ^{99m}Tc-HYNIC-Annexin V. Additionally, we would like to thank Gayatri Gowrishankar, Carmel Chan and Adam Shuhendler for insightful discussion and John Ronald for assistance with image analysis. The authors would like to acknowledge the SCi3 Small Animal Imaging Service Center, which was used to create data presented in this study, specifically, Tim Doyle for assistance with SPECT acquisition. The SCi3 Small Animal Imaging Service Center is supported by NCI grants 1P50CA114747 (ICMIC P50) and CA124435-02 (Cancer Center P30). The ML-10 precursor was supplied from GE Healthcare. We would like to acknowledge funding support from NCI ICMIC P50 CA114747 and the Ben and Catherine Ivy Foundation.

REFERENCES

1. Eisenhauer EA, Therasse P, Bogaerts J, Schwartz LH, Sargent D, Ford R, et al. New response evaluation criteria in solid tumours: revised RECIST guideline (version 1.1). Eur J Cancer. 2009;45:228-47.

2. Yang JC, Haworth L, Sherry RM, Hwu P, Schwartzentruber DJ, Topalian SL, et al. A randomized trial of bevacizumab, an anti-vascular endothelial growth factor antibody, for metastatic renal cancer. N Engl J Med. 2003;349:427-34.

3. Kreuzaler P, Watson CJ. Killing a cancer: what are the alternatives? Nat Rev Cancer. 2012;12:411-24.

4. Evan GI, Vousden KH. Proliferation, cell cycle and apoptosis in cancer. Nature. 2001;411:342-8.

5. Sellers WR, Fisher DE. Apoptosis and cancer drug targeting. J Clin Invest. 1999;104:1655-61.

6. Neves AA, Brindle KM. Imaging cell death. J Nucl Med. 2014;55:1-4.

7. Nguyen QD, Smith G, Glaser M, Perumal M, Arstad E, Aboagye EO. Positron emission tomography imaging of drug-induced tumor apoptosis with a caspase-3/7 specific [18F]-labeled isatin sulfonamide. Proc Natl Acad Sci U S A. 2009;106:16375-80.

8. Shen B, Jeon J, Palner M, Ye D, Shuhendler A, Chin FT, et al. Positron emission tomography imaging of drug-induced tumor apoptosis with a caspase-triggered nanoaggregation probe. Angew Chem Int Ed Engl. 2013;52:10511-4.

9. Blankenberg FG, Katsikis PD, Tait JF, Davis RE, Naumovski L, Ohtsuki K, et al. Imaging of apoptosis (programmed cell death) with 99mTc annexin V. J Nucl Med. 1999;40:184-91.

10. Zhao M, Li Z, Bugenhagen S. 99mTc-labeled duramycin as a novel phosphatidylethanolamine-binding molecular probe. J Nucl Med. 2008;49:1345-52.

11. Segawa K, Kurata S, Yanagihashi Y, Brummelkamp TR, Matsuda F, Nagata S. Caspase-mediated cleavage of phospholipid flippase for apoptotic phosphatidylserine exposure. Science. 2014;344:1164-8.

12. Day SE, Kettunen MI, Gallagher FA, Hu DE, Lerche M, Wolber J, et al. Detecting tumor response to treatment using hyperpolarized 13C magnetic resonance imaging and spectroscopy. Nat Med. 2007;13:1382-7.

13. Witney TH, Kettunen MI, Day SE, Hu DE, Neves AA, Gallagher FA, et al. A Comparison between Radiolabeled Fluorodeoxyglucose Uptake and Hyperpolarized C-13-Labeled Pyruvate Utilization as Methods for Detecting Tumor Response to Treatment. Neoplasia. 2009;11:574-U88.

14. Gallagher FA, Kettunen MI, Hu DE, Jensen PR, Zandt RI, Karlsson M, et al. Production of hyperpolarized [1,4-13C2]malate from [1,4-13C2]fumarate is a marker of cell necrosis and treatment response in tumors. Proc Natl Acad Sci U S A. 2009;106:19801-6.

15. Witney TH, Kettunen MI, Hu DE, Gallagher FA, Bohndiek SE, Napolitano R, et al. Detecting treatment response in a model of human breast adenocarcinoma using hyperpolarised [1-C-13]pyruvate and [1,4-C-13(2)]fumarate. British Journal of Cancer. 2010;103:1400-6.

16. Sinkus R, Van Beers BE, Vilgrain V, DeSouza N, Waterton JC. Apparent diffusion coefficient from magnetic resonance imaging as a biomarker in oncology drug development. Eur J Cancer. 2012;48:425-31.

17. Avril N, Sassen S, Schmalfeldt B, Naehrig J, Rutke S, Weber WA, et al. Prediction of response to neoadjuvant chemotherapy by sequential F-18-fluorodeoxyglucose positron emission tomography in patients with advanced-stage ovarian cancer. J Clin Oncol. 2005;23:7445-53.

18. Schelling M, Avril N, Nahrig J, Kuhn W, Romer W, Sattler D, et al. Positron emission tomography using [(18)F]Fluorodeoxyglucose for monitoring primary chemotherapy in breast cancer. J Clin Oncol. 2000;18:1689-95.

19. Spaepen K, Stroobants S, Dupont P, Van Steenweghen S, Thomas J, Vandenberghe P, et al. Prognostic value of positron emission tomography (PET) with fluorine-18 fluorodeoxyglucose ([18F]FDG) after first-line chemotherapy in non-Hodgkin's lymphoma: is [18F]FDG-PET a valid alternative to conventional diagnostic methods? J Clin Oncol. 2001;19:414-9.

20. Weber WA, Petersen V, Schmidt B, Tyndale-Hines L, Link T, Peschel C, et al. Positron emission tomography in non-small-cell lung cancer: prediction of response to chemotherapy by quantitative assessment of glucose use. J Clin Oncol. 2003;21:2651-7.

21. Wahl RL, Jacene H, Kasamon Y, Lodge MA. From RECIST to PERCIST: Evolving Considerations for PET response criteria in solid tumors. J Nucl Med. 2009;50 Suppl 1:122S-50S.

22. Grimberg H, Levin G, Shirvan A, Cohen A, Yogev-Falach M, Reshef A, et al. Monitoring of tumor response to chemotherapy in vivo by a novel small-molecule detector of apoptosis. Apoptosis. 2009;14:257-67.

23. Reshef A, Shirvan A, Waterhouse RN, Grimberg H, Levin G, Cohen A, et al. Molecular imaging of neurovascular cell death in experimental cerebral stroke by PET. J Nucl Med. 2008;49:1520-8.

24. Hoglund J, Shirvan A, Antoni G, Gustavsson SA, Langstrom B, Ringheim A, et al. 18F-ML-10, a PET tracer for apoptosis: first human study. J Nucl Med. 2011;52:720-5.

25. Hoebers FJ, Kartachova M, de Bois J, van den Brekel MW, van Tinteren H, van Herk M, et al. 99mTc Hynic-rh-Annexin V scintigraphy for in vivo imaging of apoptosis in patients with head and neck cancer treated with chemoradiotherapy. Eur J Nucl Med Mol Imaging. 2008;35:509-18.

26. Belhocine T, Steinmetz N, Hustinx R, Bartsch P, Jerusalem G, Seidel L, et al. Increased uptake of the apoptosis-imaging agent (99m)Tc recombinant human Annexin V in human tumors after one course of chemotherapy as a predictor of tumor response and patient prognosis. Clin Cancer Res. 2002;8:2766-74.

27. Reshef A, Shirvan A, Akselrod-Ballin A, Wall A, Ziv I. Small-molecule biomarkers for clinical PET imaging of apoptosis. J Nucl Med. 2010;51:837-40.

28. Witney TH, Fortt RR, Aboagye EO. Preclinical assessment of carboplatin treatment efficacy in lung cancer by 18F-ICMT-11-positron emission tomography. PLoS One. 2014;9:e91694.

29. Larkin TJ, Canuto HC, Kettunen MI, Booth TC, Hu DE, Krishnan AS, et al. Analysis of image heterogeneity using 2D Minkowski functionals detects tumor responses to treatment. Magn Reson Med. 2014;71:402-10.

30. Ardizzoni A, Boni L, Tiseo M, Fossella FV, Schiller JH, Paesmans M, et al. Cisplatin-versus carboplatin-based chemotherapy in first-line treatment of advanced non-small-cell lung cancer: an individual patient data meta-analysis. J Natl Cancer Inst. 2007;99:847-57.

31. Coiffier B, Lepage E, Briere J, Herbrecht R, Tilly H, Bouabdallah R, et al. CHOP chemotherapy plus rituximab compared with CHOP alone in elderly patients with diffuse large-B-cell lymphoma. N Engl J Med. 2002;346:235-42.

32. Cohen A, Shirvan A, Levin G, Grimberg H, Reshef A, Ziv I. From the Gla domain to a novel small-molecule detector of apoptosis. Cell Res. 2009;19:625-37.

33. Ben-Haim S, Ell P. 18F-FDG PET and PET/CT in the evaluation of cancer treatment response. J Nucl Med. 2009;50:88-99.

34. Strauss LG. Fluorine-18 deoxyglucose and false-positive results: a major problem in the diagnostics of oncological patients. Eur J Nucl Med. 1996;23:1409-15.

35. Yamane T, Daimaru O, Ito S, Yoshiya K, Nagata T, Ito S, et al. Decreased 18F-FDG uptake 1 day after initiation of chemotherapy for malignant lymphomas. J Nucl Med. 2004;45:1838-42.

36. Spaepen K, Stroobants S, Dupont P, Bormans G, Balzarini J, Verhoef G, et al. [(18)F]FDG PET monitoring of tumour response to chemotherapy: does [(18)F]FDG uptake correlate with the viable tumour cell fraction? Eur J Nucl Med Mol Imaging. 2003;30:682-8.

37. Alam IS, Neves AA, Witney TH, Boren J, Brindle KM. Comparison of the C2A Domain of Synaptotagmin-I and Annexin-V As Probes for Detecting Cell Death. Bioconjugate Chemistry. 2010;21:884-91.

38. Blankenberg FG, Vanderheyden JL, Strauss HW, Tait JF. Radiolabeling of HYNIC-annexin V with technetium-99m for in vivo imaging of apoptosis. Nat Protoc. 2006;1:108-10.

39. Grafstrom J, Stone-Elander S. Comparison of methods for evaluating radiolabelled Annexin A5 uptake in pre-clinical PET oncological studies. Nucl Med Biol. 2014.

40. Hu S, Kiesewetter DO, Zhu L, Guo N, Gao H, Liu G, et al. Longitudinal PET imaging of doxorubicin-induced cell death with 18F-Annexin V. Mol Imaging Biol. 2012;14:762-70.

41. Ye D, Shuhendler AJ, Cui L, Tong L, Tee SS, Tikhomirov G, et al. Bioorthogonal cyclization-mediated in situ self-assembly of small-molecule probes for imaging caspase activity in vivo. Nat Chem. 2014;6:519-26.

42. Nguyen QD, Lavdas I, Gubbins J, Smith G, Fortt R, Carroll LS, et al. Temporal and spatial evolution of therapy-induced tumor apoptosis detected by caspase-3-selective molecular imaging. Clin Cancer Res. 2013;19:3914-24.

43. Challapalli A, Kenny LM, Hallett WA, Kozlowski K, Tomasi G, Gudi M, et al. 18F-ICMT-11, a caspase-3-specific PET tracer for apoptosis: biodistribution and radiation dosimetry. J Nucl Med. 2013;54:1551-6.

44. Glaser M, Goggi J, Smith G, Morrison M, Luthra SK, Robins E, et al. Improved radiosynthesis of the apoptosis marker 18F-ICMT11 including biological evaluation. Bioorg Med Chem Lett. 2011;21:6945-9.

FIGURES

FIGURE 1

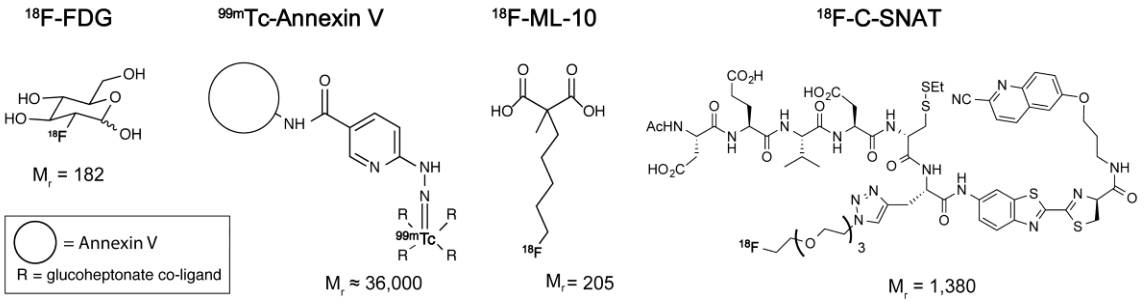

FIGURE 1. Chemical structure and molecular weight for ^{18}F-FDG, ^{99m}Tc-Annexin V, ^{18}F-ML-10 and ^{18}F-C-SNAT. The radioisotope is shown in bold type.

FIGURE 2

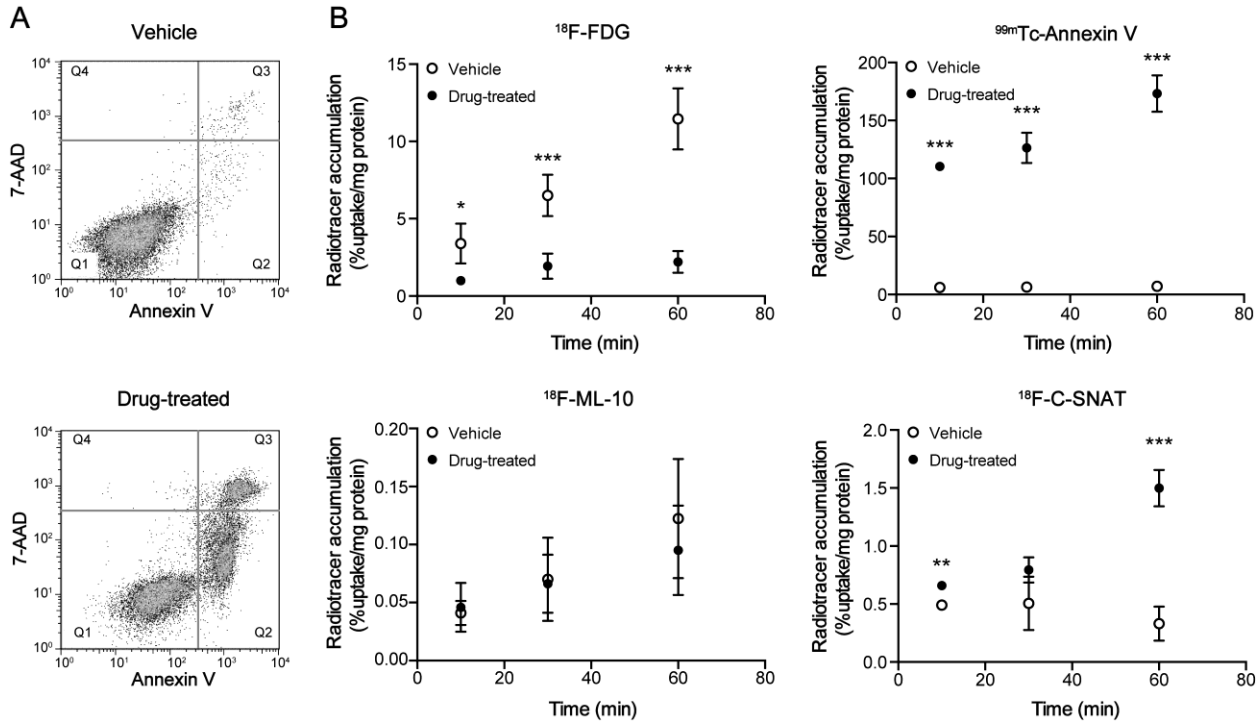

FIGURE 2. Time course of radiotracer uptake and retention in etoposide- and vehicle-treated EL-4 cells. (**A**) Flow cytometric analysis of vehicle or drug-treated (15µM etoposide; 18h) EL-4 cells. Cell death was detected with FITC-Annexin V (λ Ex/Em = 488/535) and 7-AAD staining

(λ Ex/Em = 488/647). Q1 = viable; Q2 = early apoptotic; Q3 = late apoptotic/necrotic. (**B**) Temporal changes in cell-associated radioactivity in 18h vehicle or etoposide-treated cells were measured with ^{18}F-FDG, ^{99m}Tc-HYNIC-Annexin V, ^{18}F-ML-10 and ^{18}F-C-SNAT. Mean ± SD (*n* = 3-4/group). * $P < 0.05$, ** $P < 0.01$, *** $P < 0.001$.

FIGURE 3

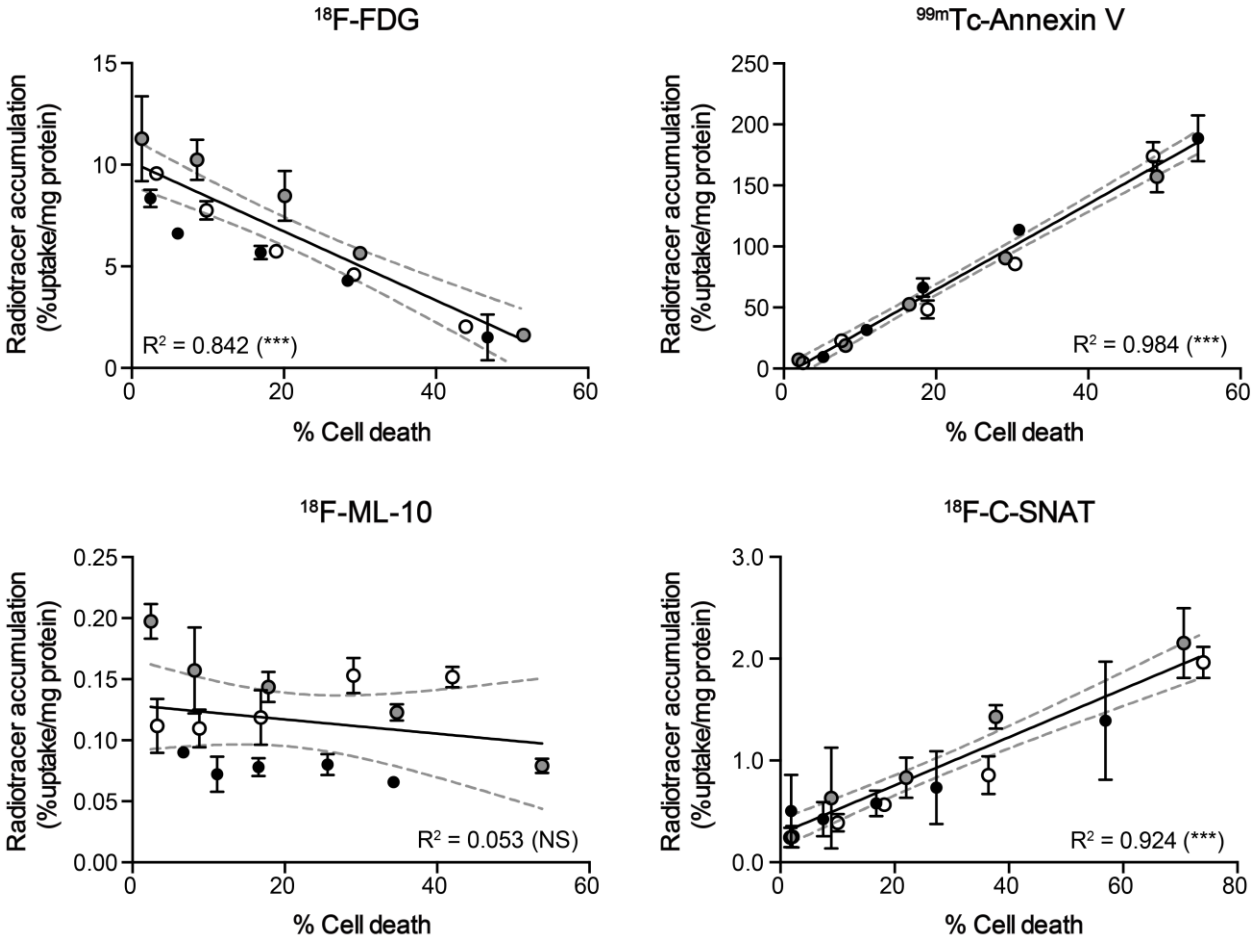

FIGURE 3. Correlation between therapy-induced cell death and radiotracer accumulation in cells. Flow cytometic quantitation of cell death was compared to cell-associated radioactivity for ^{18}F-FDG, ^{99m}Tc-HYNIC-Annexin V, ^{18}F-ML-10 and ^{18}F-C-SNAT in cell mixtures. Lines of linear regression and 95% confidence levels (broken gray lines) are shown. Mean ± SD (*n* = 3

independent experiments). Experiments performed on separate days are represented by either gray, open, or filled circles. *** $P < 0.001$; NS, not significant.

FIGURE 4

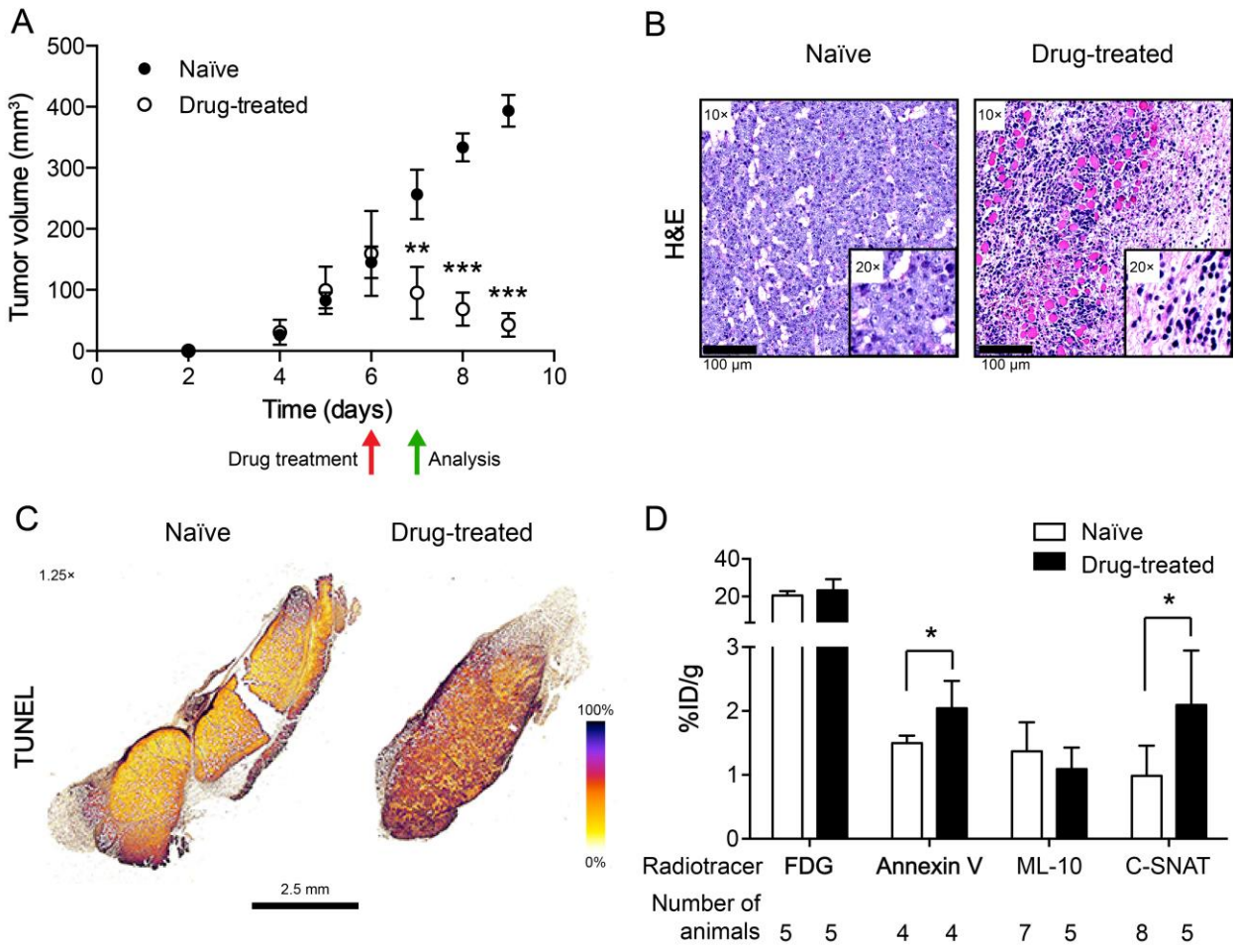

FIGURE 4. Characterization of therapy response and correlation to radiotracer accumulation in tumors. (**A**) Caliper measurements of EL-4 tumor volumes in naïve and drug-treated mice. Measurements were recorded as a function of time post cell implantation, with mice treated on day 6 (red arrow). All subsequent analysis was made on day 7, 24h post therapy (green arrow). Data represents mean ± SEM (*n* = 7-8 mice/group). (**B**) H&E staining of naïve and drug-treated histological tumor sections. Tumor sections were scanned by a whole-slide scanner, with representative regions of interest selected at 10× and 20× magnification (*insert*), indicating loss

of cellularity and immune cell infiltration following treatment (day 7, 24h post drug). Scale bar = 100 µm. (**C**) DNA fragmentation (colorimetric TUNEL assay) detection in naïve and drug-treated whole tumor sections. Representative false-color sections are shown, acquired at 1.25× magnification (scale bar = 2.5 mm). (**D**) Radiotracer accumulation in drug-treated and naïve tumors. Radioactivity was measured by γ-counting of excised tumors 90 min post radiotracer administration. The values are the mean value ± SD of at least 4 mice (number of mice shown on graph).

FIGURE 5

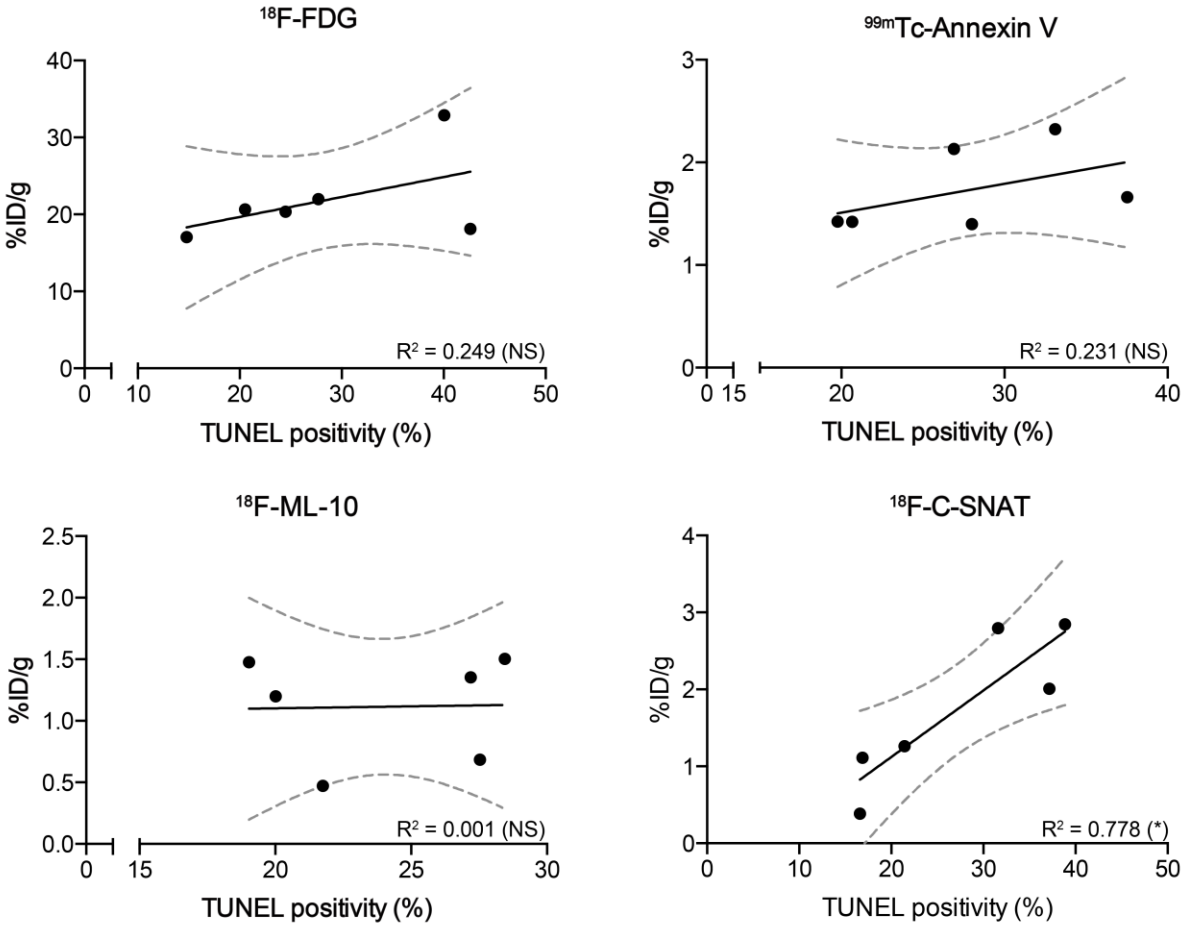

FIGURE 5. Correlation of radiotracer uptake to histological measure of tumor cell death. DNA damage, assessed by TUNEL staining of whole tumor sections (*n* = 6 sections per tumor, 3

tumors/treatment group), were compared to tumor-associated ^{18}F-FDG, ^{99m}Tc-HYNIC-Annexin V, ^{18}F-ML-10 and ^{18}F-C-SNAT radioactivity measured in tumors. Radioactivity was measured by γ-counting of excised tumors 90 min post radiotracer administration (n = 3 tumors/group). Lines of linear regression and 95% confidence levels (broken gray lines) are shown. * $P < 0.05$, ** $P < 0.01$, *** $P < 0.001$.

FIGURE 6

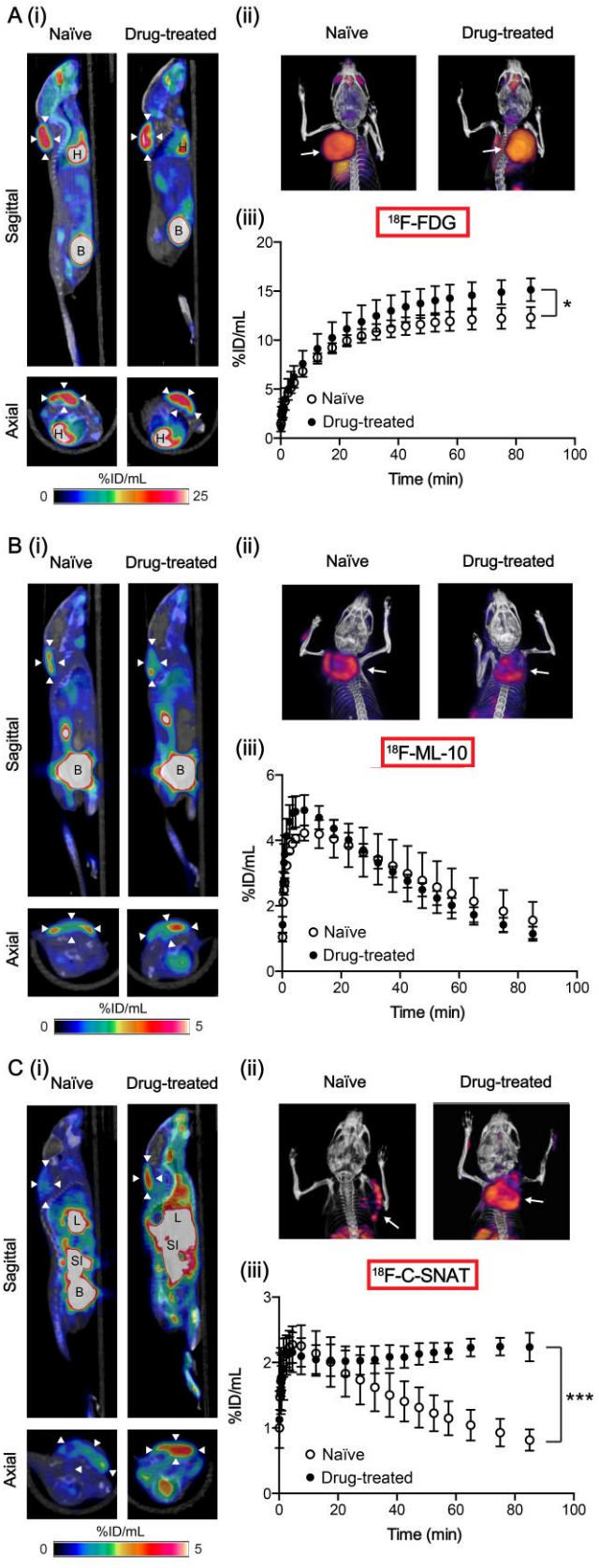
A (i)
Naïve
Drug-treated
Sagittal
Axial
H
B
%ID/mL
0
25
(ii)
Naïve
Drug-treated
(iii)
18F-FDG
%ID/mL
Naïve
Drug-treated
Time (min)
*
B (i)
Naïve
Drug-treated
Sagittal
Axial
B
%ID/mL
0
5
(ii)
Naïve
Drug-treated
(iii)
18F-ML-10
%ID/mL
Naïve
Drug-treated
Time (min)
C (i)
Naïve
Drug-treated
Sagittal
Axial
L
SI
B
%ID/mL
0
5
(ii)
Naïve
Drug-treated
(iii)
18F-C-SNAT
%ID/mL
Naïve
Drug-treated
Time (min)
***

FIGURE 6. Dynamic PET imaging of cell death *in vivo*. PET image analysis of EL-4 tumors in naïve and drug-treated mice was performed for ^{18}F-FDG (**A**), ^{18}F-ML-10 (**B**) and ^{18}F-C-SNAT (**C**). Corresponding axial and sagittal PET-CT images (60 – 90 min summed activity) of naïve and drug-treated EL-4 tumor-bearing mice are shown in panels (**i**). Arrowheads indicate the tumor, identified from the CT image. (**ii**) Representative PET-CT (60 – 90 min summed activity) volume rendering technique (VRT) images of tumor-bearing naïve and drug-treated mice. Arrows indicate the tumor. (**iii**) The tumor time-activity curves (TAC) representing average counts from a dynamic 90-minute scan 24h post drug treatment and in naïve animals. Data are mean ± SD (n = 3 – 4 animals per group). * $P < 0.05$, *** $P < 0.001$. B = bladder, H = heart, L = liver, SI = small intestine.